Fano Effects and Wave Functions in a Quantum Dot

Takeshi NAKANISHI[1], Kiyoyuki TERAKURA[1,2], and Tsuneya ANDO[3]

[1] *National Institute of Advanced Industrial Science and Technology, 1 Umezono, Tsukuba 305-8568, Japan*
[2] *Creative Research Initiative "Sousei", Hokkaido University, Kita 21, Nishi 10, Kita-ku, Sapporo 001-0021, Japan*
[3] *Department of Physics, Tokyo Institute of Technology, 2-12-1 Ookayama, Meguro-ku, Tokyo 152-8551, Japan*

The analysis of wave functions shows that states in a quantum dot embedded in an Aharonov-Bohm ring are classified into two groups, a large number of weekly coupled states and a small number of strongly coupled states. Coexistence of these states leads to a phase persistence in the Fano and Aharonov-Bohm effects, which has been observed in experiments.

KEYWORDS: Fano Effect, Aharonov-Bohm Effect, Several Channels, Recursive Green's Function Technique, Coulomb Blockade, Quantum Dot

1. INTRODUCTION

In an Aharonov-Bohm (AB) ring containing a quantum dot, a series of consecutive conductance peaks with a Fano type interference with similar asymmetry and phase of an AB oscillation have been observed.[1,2] A Fano-type lineshape was reported also in a weakly coupled single quantum dot.[3,4] The purpose of this work is to theoretically explore Fano resonances in a realistic model through the analysis of wavefunctions in the quantum dot for the purpose of understanding some of interesting experimental findings.

In earlier experiments, AB oscillations were observed in an AB ring with a quantum dot and the phase of the oscillation was shown to change by π across a resonance peak.[5–8] A surprising and unexpected finding is that the phase becomes the same between adjacent peaks, showing that it has to change by another π between those peaks. Since then, various theoretical studies have been reported on the phase of the AB oscillation and the Fano effect within one-dimensional (1D) models in which the AB ring consists of a chain.[9–18]

It was suggested, for example, that because the Friedel sum rule leading to a π change across a peak is still valid in the presence of a Fano-type interference, the extra π change between neighboring peaks is likely to be due to hidden electron charging events that do not cause conductance peaks.[10] The possible disappearance of some peaks due to an interference inside the AB ring[11] and the vanishing of the transmission coefficient occurring in a 1D model due to the Fano-type interference[14] were suggested as possible candidates for the mechanism giving rise to such an extra phase change. A mechanism giving rise to the extra π phase-change between neighboring peaks in a near chaotic dot is provided,[15] and an effects of lossy channels is discussed in the Aharonov-Bohm ring.[16]

Since the more recent observation of a clear Fano effect,[1] various calculations were made further, including those in a 1D model[17,18] and in a realistic model.[19] In particular, the phase persistence of AB and Fano effects has been qualitatively reproduced in the latter calculation.[19] In the model, the AB ring contains several conducting channels and a quantum dot with dimensions comparable to those in the experiments. The coexistence of a small number of strongly coupled states and many weakly coupled states in the dot with finite width has been suggested to be responsible for the phase persistence.

In this work, we calculate wave functions in the quantum dot with the use of the same model and confirm this suggestion. The organization of the paper is as follows: After introducing the realistic model in Sec. II, numerical results are shown in Sec. III. Discussion on the relation to experiments is given in Sec. IV and a summary and conclusion are given in Sec. V.

2. Model and Method

We use a model of the AB ring with radius a, straight up and down arms with length L, a quantum dot with length L_D in the down arm separated by wall barriers with length L_W, and a control gate with length L_W as shown in Fig. 1. The strength of a magnetic field applied perpendicular to the AB ring is characterized by ϕ/ϕ_0, where ϕ is magnetic flux passing through the stadium with area $aL + \pi a^2/4$ and ϕ_0 is the magnetic flux quantum given by $\phi_0 = ch/e$.

To construct the model potential, we first consider a hexagon defined by six vertices at $\mathbf{r} = \pm\mathbf{a}/2$, $\pm\mathbf{b}/2$, and $\pm(\mathbf{a}-\mathbf{b})/2$ with $\mathbf{a} = (\sqrt{3}/2, 1/2)a$ and $\mathbf{b} = (0,1)a$ and define an antidot potential which vanishes outside the hexagon and is given by

$$v_{\rm antidot}(\mathbf{r}) = u_0 \left| \cos\left(\frac{\pi \mathbf{a}\cdot\mathbf{r}}{a^2}\right) \cos\left(\frac{\pi \mathbf{b}\cdot\mathbf{r}}{a^2}\right) \cos\left(\frac{\pi (\mathbf{a}-\mathbf{b})\cdot\mathbf{r}}{a^2}\right) \right|^{4/3}, \quad (1)$$

inside the hexagon. This potential was used in previous studies on transport properties of antidot lattices.[20]

We consider next the rectangular region near the top-right corner as shown in Fig. 1 and define the origin $\mathbf{r} = 0$ at the bottom-left corner of this region. The rectangle is divided into four different regions denoted by I, II, III, and IV by dotted lines. The region I is defined by $y < x/\sqrt{3}$ and $y < -\sqrt{3}x + a$, the region II is defined by $y < x/\sqrt{3}$ and $y > -\sqrt{3}x + a$, and the region IV is defined by $\sqrt{x^2+y^2} > 2a$. The potential is defined by $v(\mathbf{r}) = v_{\rm antidot}(\mathbf{r})$ in I, $v(\mathbf{r}) = v_{\rm antidot}(\mathbf{r}-\mathbf{a})$ in II, and $v(\mathbf{r}) = u_0$ in region IV. In region III the potential along the line $y = x/\sqrt{3}$ of the regions I and II is rotated around the origin. The potential in the up arm is the

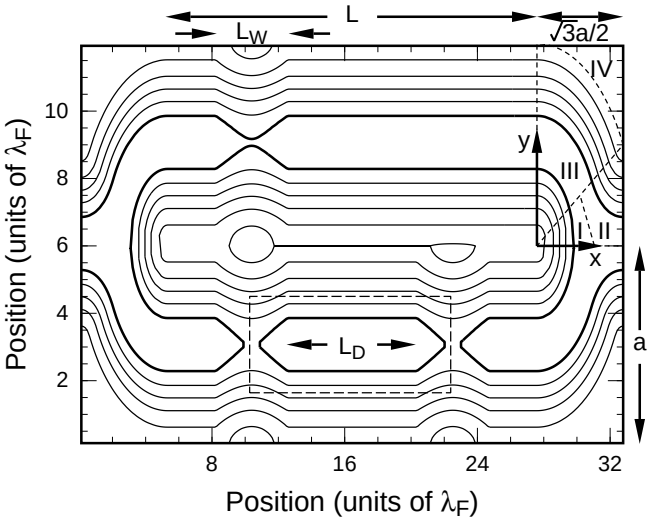

Fig. 1. Equi-potential lines of the model AB ring with a dot, plotted with energy interval of Fermi energy E_F. The thick lines correspond to the Fermi energy. In this example $V_g/E_F = 0$, $V_c/E_F = 0.95$, and $W/E_F = 1.03$. The rectangular region near the top-right corner is separated into four regions I, II, III, and IV. The rectangular region denoted by dashed lines covering the dot in the lower arm denoted is used for estimating the width of the wave function in the dot.

same as that along $x = 0$ of the region III. The potential in the rectangular regions near other corners and in the down arm are defined in a symmetric way. Two ideal leads with a uniform cross section same as that in the up and down arms are continuously connected to the left and right entrances of the AB ring.

The wall potential separating the dot from the arm is defined as

$$V(\mathbf{r}) = W \cos\Big(\frac{\pi x}{L_W}\Big), \tag{2}$$

for $-L_W/2 < x < L_W/2$ and $-a < y < 0$, where an origin of x is chosen at the center of each wall. The potential of the control gate is given by the same expression for $-L_W/2 < x < L_W/2$ and $0 < y < a$ except that the height W is replaced by V_c. They are superposed on the potential of the AB ring. A gate potential V_g is uniformly applied in the dot in the region of $-a < y < 0$ with length L_D.

For a realistic quantum dot embedded in the AB ring, the adiabatic conditions are nearly satisfied, i.e., $|dD(x)/dx| \ll 1$ and $|D(x)d^2D(x)/dx^2| \ll 1$ with $D(x)$ being the width of the wave-guide at the Fermi energy E_F. Therefore, we choose $L_W/\lambda_F = 5$ with Fermi wave length λ_F. Calculations of transmission and reflection probabilities for the single wall with height $W \lesssim E_F$ reveal that essentially electrons in the lowest 1D subband with the highest velocity in the incident direction can get over the wall and there is very little mixing between different 1D subbands or channels. In order to simulate actual situations, further, we introduce a weak random potential in the dot. The amount of the disorder corresponds to a mean free path of $10\times\lambda_F$ or level broadening of $0.015\times E_F$ in the two-dimensional system.

We use some fixed parameters in numerical calculations, $W/E_F = 1.03$, the ring radius $a/\lambda_F = 6$, the arm length $L/\lambda_F = 20.8$, and the width of arms and leads $1.8\times\lambda_F$ at the Fermi energy, which results in $u_0/E_F = 5.44$. In comparison with the geometry of the actual experiments for which $\lambda_F = 40$ nm,[1] the system size is roughly half except for L_D of a comparable length. There are three sets of the traveling modes in the arms and leads, which can describe the actual feature of the experiment in which there are several channels. Further, we shall consider the magnetic flux around $\phi/\phi_0 = 80$ corresponding to 1.3 T, which is typical magnetic field in the experiments.

A self-consistent calculation in quantum wires fabricated at GaAs/AlGaAs heterostructures suggests that the potential is nearly parabolic for a wire with small width, but consists of a flat central region and a parabolic increase near the edge for a wider wire.[21,22] In the above the exponent 4/3 in $v_{\rm antidot}(\mathbf{r})$ has been chosen in such a way that the total exponent of cosine function becomes 4, for which the potential gradient at the Fermi energy corresponds to that of such a realistic confinement potential. The model is essentially same as that described in a previous study apart from the presence of the dot and the control gate.[20]

The conductance is calculated by the use of the Landauer formula

$$G = \frac{e^2}{\pi\hbar}\sum_{jj'}|t_{jj'}|^2, \tag{3}$$

where $t_{jj'}$ is the transmission coefficient for a wave incoming from the j'th channel in the left lead and outgoing to the jth channel in the right.[23] The summation is taken over all traveling modes in the leads. To calculate $t_{jj'}$, we use recursive Green's function technique on the lattice model with a lattice constant a'.[24] For explicit numerical calculations we choose $\lambda_F/a' = 7$.

3. Fano Peaks and Dot States

We consider the case where the up arm is nearly pinched off by the control gate. In this case the situation is close to that of so-called double slit experiments, because the transmission probability of an electron passing through the up arm is small and not so much different from that through the down arm and therefore multiple scattering in the AB ring is less important.

Figure 2 (a) shows an example of the calculated conductance as a function of the gate potential for the control gate $V_c/E_F = 1$ and $\phi/\phi_0 = 80$. Many peaks appear in the conductance, but they can be classified into two groups, small numbers of wide peaks with large broadening and large numbers of narrow peaks. In this example, the wide peaks are at $V_g/E_F = -0.18$, -0.06, 0.07, and 0.18 indicated by arrows in the figure. All resonance peaks in the conductance are asymmetric with a dip in the right or left side. This asymmetry is due to interference of the waves passing through the up arm and transmitted resonantly through the dot in the down arm, i.e., the so-called Fano interference.

In order to analyze such interference effects including the AB oscillation, we first consider transmission coeffi-

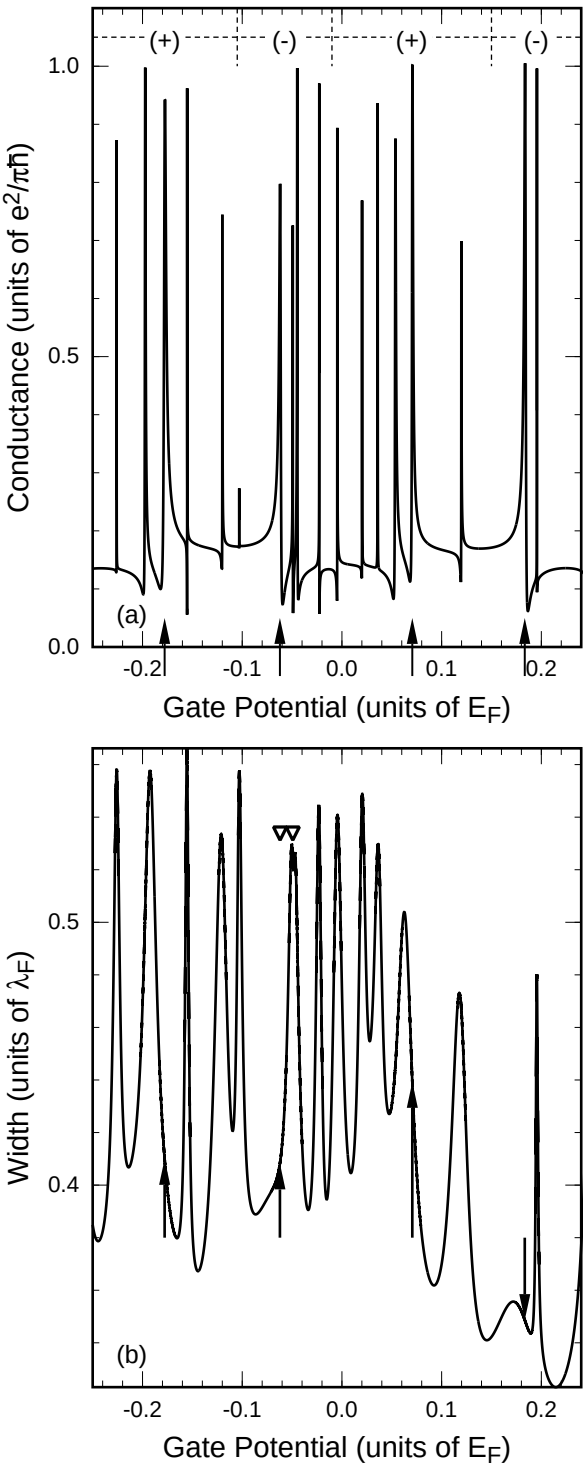

Fig. 2. (a) Fano resonances in the calculated conductance at both wide and narrow peaks for flux $\phi/\phi_0 = 80$. The arrows indicate the position of the wide peaks when the up arm is pinched off. The region for positive and negative values of the asymmetry parameter q' are also shown by (+) and (−), respectively. (b) A width of the wavefunction in the dashed rectangle in Fig. 1 as a function of energy. The vertical arrows indicate the energies corresponding to the wide peaks in (a) and the inverted triangles show energies for which the actual wave function is shown in Fig. 3.

cients $t^d_{jj'}$ through a quantum dot embedded in a straight wave-guide. In the vicinity of a dot level with energy E_ν, the transmission coefficient through the dot is given by

$$t^d_{jj'} = \frac{-2\pi i V_{j\nu}(E) V_{\nu j'}(E) D(E)}{E - E_\nu - F_\nu + i\Gamma_\nu}, \tag{4}$$

where $V_{j\nu}(E)$ and $V_{\nu j'}(E)$ are the matrix elements of transitions from the dot state to the out-going states and from the incident to the dot state, respectively, $D(E)$ is the density of states in each wave-guide, and

$$\begin{aligned} F_\nu &= \mathrm{P}\int \frac{|V_\nu(E')|^2}{E' - E_\nu} D(E') dE', \\ \Gamma_\nu &= \pi |V_\nu(E)|^2 D(E), \end{aligned} \tag{5}$$

with $|V_\nu(E')|^2$ being the total intensity of the transition between the dot and the left and right wave-guides. This is rewritten as

$$t^d_{jj'} = \frac{\alpha_{jj'}}{\epsilon + i}, \tag{6}$$

with

$$\begin{aligned} \alpha_{jj'} &= -2\pi i V_{j\nu}(E) V_{\nu j'}(E) D(E) \Gamma_\nu^{-1}, \\ \epsilon &= (E - E_\nu - F_\nu)\Gamma_\nu^{-1}. \end{aligned} \tag{7}$$

The transmission probabilities exhibit a resonance with the conventional Breit-Wigner lineshape.

When the double-slit condition is valid, the transmission through the AB ring incoming from the j'th channel in the left lead and out-going to the jth channel in the right lead is given by

$$t_{jj'} = t^0_{jj'} + t^d_{jj'}, \tag{8}$$

where $t^0_{jj'}$ is a transmission coefficient for the up arm, essentially independent of energy in the energy scale determined by Γ_ν. Effects of scattering at entrances of the AB ring can be absorbed in the coefficients $\alpha_{jj'}$ for $t^d_{jj'}$. The total transmission probability is written as

$$|t_{jj'}|^2 = |t^0_{jj'}|^2 \frac{|\epsilon + q_{jj'}|^2}{\epsilon^2 + 1}, \tag{9}$$

with a complex Fano parameter

$$q_{jj'} = \frac{\alpha_{jj'}}{t^0_{jj'}} + i. \tag{10}$$

As a result, the total conductance is given by

$$G = \frac{e^2}{\pi\hbar} \sum_{j,j'} |t_{jj'}|^2 = \frac{e^2}{\pi\hbar} T_0 \frac{|\epsilon + q|^2}{\epsilon^2 + 1}, \tag{11}$$

with a complex Fano parameter $q = q' + iq''$ and a parameter T_0, which are given by

$$\begin{aligned} T_0 &= \sum_{jj'} |t^0_{jj'}|^2, \\ q' &= T_0^{-1} \sum_{jj'} |t^0_{jj'}|^2 q'_{jj'}, \\ (q'')^2 &= T_0^{-1} \sum_{jj'} |t^0_{jj'}|^2 [(q'_{jj'})^2 + (q''_{jj'})^2] - (q')^2. \end{aligned} \tag{12}$$

The real part q' of q determines the asymmetry of the conductance lineshape, i.e., a dip appears in the left hand

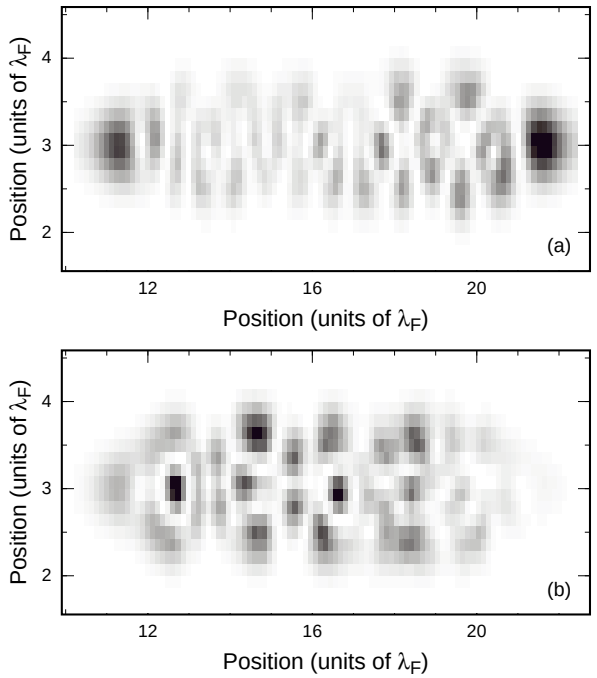

Fig. 3. Calculated squared amplitude of the wave function for (a) a wide peak at $V_g/E_F = -0.062$ and (b) a narrow peak at $V_g/E_F = -0.049$ in the dashed rectangular region in Fig. 1. The corresponding gate voltages are pointed by triangles in Fig. 2 (b).

side of a peak for positive q' and in the right hand side for negative q'.

Figure 2 (a) shows that q' changes sign alternately when the gate potential crosses wide peaks denoted by arrows. For the narrow peaks, on the other hand, the sign of q' does not show such an alternate change from peak to peak but follows the sign of the nearest wide peaks. In fact, four narrow peaks in the range $-0.11 < V_g/E_F < -0.01$ have a dip in the right side of peaks, in agreement with the behavior of the wide peak at -0.06. Further, five narrow peaks in $-0.01 < V_g/E_F < 0.13$ have a dip in the left side of the peak again following the nearest wide peak at 0.07. In Fig. 2 (a) the sign of q' of narrow peaks is denoted by (+) and (−).

In the adiabatic limit, where the confinement potential varies slowly in the scale of the Fermi wave length, each one-dimensional channel has its own effective potential and mixing between different channels are small. Therefore, the transmissions through dot states with the same 1D subband index are possible and in particular those associated with the lowest subband having the largest kinetic energy in the wave-guide direction contribute to transmissions because of the lowest effective tunneling barrier. The wide resonances shown in Fig. 2 (a) actually correspond to such states.

The selection rule is violated slightly due to the deviation from the adiabatic limit and also by the presence of unavoidable disorder. Let $\hat{H}'$ be the Hamiltonian describing effects of such deviation, ψ_n^0 be a dot state uncoupled to wave-guide states in the absence of $\hat{H}'$, and ψ_N^0 be the nearest dot state coupled to wave-guide states even in the absence of $\hat{H}'$. Then, apart from energy shift, the state ψ_n associated with ψ_n^0 now contains a contribution of ψ_N^0, i.e.,

$$\psi_n \approx \psi_n^0 + \psi_N^0 \frac{(N|\hat{H}'|n)}{E_n - E_N}, \tag{13}$$

where the lowest order energy shift has been taken into account already in energies E_n and E_N. Then, in the vicinity of E_n, the matrix element for the transmission through the dot becomes

$$V_{jn}V_{nj'} \approx V_{jN}V_{Nj'} \frac{|(N|\hat{H}'|n)|^2}{(E_n - E_N)^2}. \tag{14}$$

This shows that the phase of $V_{jn}V_{nj'}$ is given by that of $V_{jN}V_{Nj'}$ of the nearest wide peak, explaining the essential feature of the numerical result that the asymmetry of the Fano interference of narrow peaks follows that of a neighboring wide peak.

Examples of the squared amplitude of the wave function $\rho(\mathbf{r})$ are shown in Fig. 3 for (a) a wide peak at $V_g/E_F = -0.062$ and in (b) a narrow peak at $V_g/E_F = -0.049$. These values of the control gate are marked in Fig. 2 (b) by triangles. First, we should note that the large amplitude near left and right ends in Fig. 3 (a) demonstrates a large contribution to the conductance. The wave function (a) at the wide peak is less nodal and narrower in the direction perpendicular to the wave-guide direction, but has many nodes in the wave-guide direction. This shows that a large kinetic energy in the wave-guide direction and a small kinetic energy in the perpendicular direction, which is consistent with the fact that the dot state is associated with the lowest 1D subband. On the contrary, the wave function (b) at the narrow peak shows a smaller kinetic energy in the wire direction and a larger kinetic energy in the perpendicular direction, corresponding to a dot state associated with a higher 1D subband.

The nature of the wave function in the dot can be characterized by an effective width Δy, which is an extention of the wave function in y direction, defined by

$$\Delta y = \sqrt{\langle (y - \langle y \rangle)^2 \rangle}, \tag{15}$$

with

$$\langle y \rangle = \int y\rho(\mathbf{r}) d\mathbf{r} \Big(\int \rho(\mathbf{r}) d\mathbf{r} \Big)^{-1}, \tag{16}$$

where the integral is in the dashed rectangular region shown in Fig. 1.

Figure 2 (b) shows the width Δy as a function of the gate potential. The calculated width takes a sharp maximum at narrow peaks of the conductance, but does not exhibit any appreciable structure at wide peaks. Further, the width at the wide peaks does not vary so much from peak to peak and is about the same as the width of the lowest 1D subband in the wave guide. These results clearly show the validity of the assignment of narrow peaks to dot states associated to excited 1D subbands and wide peaks to those associated to the lowest subband.

When only the transport through a dot embedded in a wave-guide is possible, i.e., when the control gate is pinched off, a Fano type interference is possible between

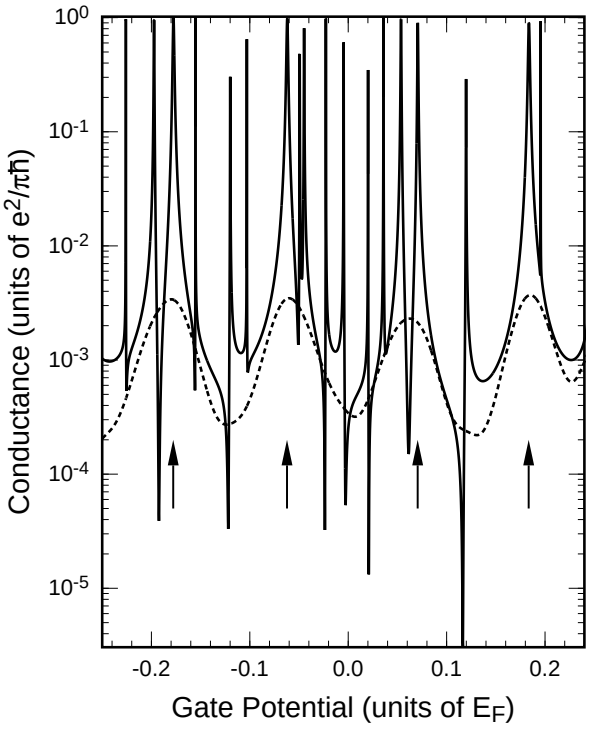

Fig. 4. Resonant peaks in the conductance in the presence of a magnetic field $\phi/\phi_0 = 80$, when the control gate is pinched off with $V_c/E_F = 2$. The conductance averaged over the gate potential with width $0.01E_F$ is shown by a dotted line. The arrows indicate the position of the wide peaks.

different processes within a dot. A nonresonant transmission through the dot state E_N becomes significant, which is ignored in the previous consideration for Fig. 2, because it is much smaller than waves passing through the up arm. In the vicinity of the resonance at a narrow peak at E_n, we have

$$t^d_{jj'} \approx -2\pi i D(E)\Big[\frac{V_{jn}V_{nj'}}{E-E_n+i\Gamma_n} + \frac{V_{jN}V_{Nj'}}{E_n-E_N}\Big] = -2\pi i D(E)\frac{V_{jN}V_{Nj'}}{E_n-E_N}\Big(\frac{|(N|\hat{H}'|n)|^2}{(E_n-E_N)(E-E_n+i\Gamma_n)}+1\Big). \quad (17)$$

This shows that the Fano interference of the resonance at E_n with the nonresonant transmission through the dot state E_N changes sign when the energy crosses E_N, i.e., $q' < 0$ and $q' > 0$ in the left and right hand side, respectively.

Figure 4 shows the calculated conductance when the up arm is pinched off with $V_c/E_F = 2$. The conductance averaged over a finite width of the gate potential is also included, which shows only the structure due to broad peaks because narrow peaks are all averaged out. For the narrow peaks, we see the Fano line-shape with a dip. In the vicinity of a wide peak, the asymmetry of narrow peaks is such that $q' < 0$ in the left hand side and $q' > 0$ in the right hand side, in agreement with the above simple approximation (Eq. (17)).

4. Discussion

In actual experiments, as the charging energy of a dot is dominant, it causes a Coulomb blockade effect and determines a typical scale of the gate potential. As has been shown in above mentioned examples, most of dot states contributing to the Coulomb oscillation are those of narrow peaks because of their dominance in the number and only a few of those of wide peaks appear. This means that the asymmetry of the Fano resonance stays the same for several consecutive narrow conductance peaks as long as they are connected with the same wide peak (Eq. (13)) and also the phase of the AB oscillation does not change among such peaks.[19)]

The asymmetry of a narrow peak changes, when the dot state contributing to the narrow peak is mixed to a different dominant wide-peak state. In the region of such crossover gate potential, the asymmetry may exhibit a complicated behavior because a dominant wide-peak state may vary from a peak to a peak. Further, the phase of the AB oscillation changes only when the gate potential crosses the wide peak.[19)] These behaviors can account for the most of the features of the experimental results (Fig. 2(a) of Ref. 1, for example).

In the absence of a random potential, the result is qualitatively same as the results given above with a few exceptions on the asymmetry of the Fano resonance of narrow peaks. Without randomness, the dot is symmetric and therefore the symmetry of the wavefunction can play important roles in causing mixing between dot levels. In fact, the exception can appear more easily, if the symmetry of wavefunction prevents a narrow level from coupling to a nearest wide level but allows to a different wide level.

5. Summary and Conclusion

We have numerically calculated the conductance and wavefunctions using a realistic model of an AB ring with a quantum dot in a down arm and a control gate in the up arm which controls the channel number. Many peaks appear in the conductance, but they can be classified into two groups, small numbers of wide peaks with large broadening and large numbers of narrow peaks. The sign of the asymmetry parameter of the Fano-type interference of narrow peaks is almost always same as that of a nearest wide peak.

When the control gate is such that the up arm is nearly pinched off, the situation is close to that of double-slit experiments, and therefore the asymmetry parameter changes at the middle of neighboring wide peaks and the phase of the AB oscillation changes by $\sim \pi$ only when the gate potential crosses the wide peak.

Most of dot states contributing to the Coulomb oscillation are those of the narrow peaks because of their dominance in the number. Consequently, the asymmetry of the Fano line-shape stays the same for the several consecutive narrow conductance peaks as long as they are connected with the same wide peak and also the phase of the AB oscillation does not change among such peaks, which explains essential features of experiments.

Acknowledgments

We thank K. Kobayashi, H. Aikawa, and S. Katsumoto for helpful discussion. This work has been supported by a NAREGI nano-science project, by a 21st Century

COE Program at Tokyo Tech "Nanometer-Scale Quantum Physics", and by Grant-in-Aid for COE (12CE2004 "Control of Electrons by Quantum Dot Structures and Its Application to Advanced Electronics") from the Ministry of Education, Science and Culture, Japan.

1) K. Kobayashi, H. Aikawa, S. Katsumoto, and Y. Iye, Phys. Rev. Lett. **88**, 256806 (2002).
2) K. Kobayashi, H. Aikawa, S. Katsumoto, and Y. Iye, Phys. Rev. B **68**, 235304 (2003).
3) J. Göres, D. Goldhaber-Gordon, S. Heemeyer, and M. A. Kastner, Phys. Rev. B **62**, 2188 (2000).
4) I. G. Zacharia, D. Goldhaber-Gordon, G. Granger, M. A. Kastner, Yu. B. Khavin, H. Shtrikman, D. Mahalu, and U. Meirav, Phys. Rev. B **64**, 155311 (2001).
5) A. Yacoby, M. Heiblum, D. Mahalu, and H. Shtrikman, Phys. Rev. Lett. **74**, 4047 (1995).
6) A. Yacoby, R. Schuster, and M. Heiblum, Phys. Rev. B **53**, 9583 (1996).
7) R. Schuster, E. Buks, M. Heiblum, D. Mahalu, V. Umansky, and H. Shtrikman, Nature **385**, 417 (1997).
8) See also, G. Hackenbroich, Phys. Reports **343**, 463 (2001).
9) Y. Gefen, Y. Imry, and M. Ya. Azbel, Phys. Rev. Lett. **52**, 129 (1984).
10) A. L. Yeyati and M. Büttiker, Phys. Rev. B **52**, R14360 (1995).
11) J. Wu, B. -L. Gu, H. Chen, W. Duan, and Y. Kawazoe, Phys. Rev. Lett. **80**, 1952 (1998).
12) H. Xu and W. Sheng, Phys. Rev. B **57**, 11903 (1998).
13) C. -M. Ryu and S. Y. Cho, Phys. Rev. B **58**, 3572 (1998).
14) H. -W. Lee, Phys. Rev. Lett. **82**, 2358 (1999).
15) P. G. Silvestrov and Y. Imry, Phys. Rev. Lett. **85**, 2565 (2000).
16) A. Aharony, O. Entin-Wohlman, B. I. Halperin, and Y. Imry, Phys. Rev. B **66**, 115311 (2002).
17) O. Entin-Wohlman, A. Aharony, Y. Imry, Y. Levinson, and A. Schiller, Phys. Rev. Lett. **88**, 166801 (2002).
18) A. Ueda, I. Baba, K. Suzuki, and M. Eto, Suppl. A to J. Phys. Soc. Jpn. **72**, 157 (2003).
19) T. Nakanishi, K. Terakura, and T. Ando, Phys. Rev. B **69**, 115307 (2004).
20) T. Nakanishi and T. Ando, Phys. Rev. B **54**, 8021 (1996); Physica B **227**, 127 (1996).
21) A. Kumar, S.E. Laux, and F. Stern, Phys. Rev. B **42**, 5166 (1990).
22) T. Suzuki and T. Ando, J. Phys. Soc. Jpn. **62**, 2986 (1993).
23) R. Landauer, IBM J. Res. Dev. **1**, 223 (1957); Phil. Mag. **21**, 863 (1970).
24) T. Ando, Phys. Rev. B **44**, 8017 (1991).